To link to this article : DOI: 10.1016/j.ces.2014.08.063
http://dx.doi.org/10.1016/j.ces.2014.08.063

Critical agitation for microcarrier suspension in orbital shaken bioreactors: Experimental study and dimensional analysis

Eric Olmos [a,b,*], Karine Loubiere [c,d], Céline Martin [a,b], Guillaume Delaplace [e], Annie Marc [a,b]

[a] CNRS Laboratoire Réactions et Génie des Procédés, UMR 7274, 2 avenue de la forêt de Haye TSA 40602, Vandoeuvre-les-Nancy, F-54518, France
[b] Université de Lorraine, LRGP, CNRS UMR 7274, 2 avenue de la forêt de Haye TSA 40602, Vandoeuvre-les-Nancy, F-54518, France
[c] CNRS, Laboratoire de Génie Chimique (LGC UMR 5503), 4 allée Emile Monso, BP 84234, F-31432 Toulouse, France
[d] Université de Toulouse, INPT, ENSIACET, F-31432 Toulouse, France
[e] INRA, Laboratoire PIHM UR 638, BP 39, F-59651 Villeneuve d'Ascq, France

HIGHLIGHTS

- Experimental characterization of particle suspension in orbital shakers.
- New correlation predicting critical agitation conditions for complete particle suspension.
- Larger orbital diameters promote smaller power dissipations at complete particle suspension.

ABSTRACT

Orbital shaken bioreactors are widely used at the laboratory scale for the culture of animal cells in suspension mode. In the case of adherent-dependent cell lines, the choice of agitation conditions at which all particles are just-suspended (or attain complete suspension) has often to be determined. Indeed, with orbital shaken bioreactors, this choice results from the combination of two parameters: the orbital diameter and the agitation rate. That is why, a new experimental protocol for the determination of critical agitation conditions for microcarrier complete suspension has been developed in this paper. It consisted in a side-view visualization of blue-stained particles in shaken Erlenmeyer flasks and cylindrical flasks. 220 experiments representative of animal cell culture conditions have been carried out to study the effect of various operating conditions (bioreactor size and geometry, particle type, density and diameter, liquid viscosity, shaking diameter, filling ratio). Furthermore, a dimensional analysis has been performed, leading to a correlation relating a Froude number (in which the critical agitation N_c for complete particle suspension is embedded) to four other dimensionless numbers. Then, the critical agitation conditions determined in this paper were analyzed and discussed with respect to the data available in the literature on the flow structure occurring inside the flask. Our findings revealed that high orbital shaking diameters and large cylindrical vessels should be promoted to get microcarriers into suspension at a minimized power dissipation per unit of volume.

Keywords:
Shaken flasks
Dimensional analysis
Microcarrier suspension
Experimental determination

1. Introduction

Adherent-dependent cell culture on microcarriers in mixed bioreactors finds many applications in the pharmaceutical industry for the production of vaccines. Other applications are now found in tissue engineering and in cell therapy, particularly for the expansion of mesenchymal stem cells (Ferrari et al., 2012). In adherent-dependent cell cultures, a particular attention has to be paid to bioreactor agitation. A too low agitation condition may lead to microcarrier settling and to the occurrence of some gradients of pH, O_2 or nutrient concentrations whereas a too vigorous mixing would lead to cell or microcarrier damage. In microcarrier cultures, hydromechanical damage arises from particle–particle collisions, impeller–microcarrier interactions and/or liquid turbulence and, especially, from turbulent eddies whose characteristic dimension is similar to microcarrier size (Cherry and Papoutsakis, 1988). Microcarrier suspension in bioreactors is generally looked for in order to avoid particle–particle contact points, and thus to increase the available adherence area for the cells and to enhance mass transfer between cells and their environment.

Hence, to define a suitable mixing strategy as well as for scale-up purposes, the critical agitation rate for particle complete

* Corresponding author.
E-mail address: eric.olmos@univ-lorraine.fr (E. Olmos).

suspension N_c (also called the just-suspended agitation rate) has to be considered and quantified: N_c refers to the minimum agitation conditions at which all particles attain complete suspension (Zwietering, 1958). The definition of the critical agitation rate for particle complete suspension relies on usual concepts in solid–liquid mixing tanks. While at low agitation rates, all particles remain settled at the bottom of the vessel, an increase of N induces the motion of a fraction of particles (partial suspension). A further increase of N reduces the number of particles settled till N_c for which no particles remain deposited more than one or two seconds approximately (complete suspension). For higher agitation rates, gradients of particle concentration are reduced towards full homogeneity (homogeneous suspension). Particle suspension is the result of complex phenomena involving turbulent eddies, forces acting on particles (drag, buoyancy, gravity), wall–particle and particle–particle interactions.

In the case of mechanically stirred bioreactors with a central impeller rotating around a vertical axis, the critical agitation rate N_c is generally predicted using the well-known Zwietering equation (Zwietering, 1958) as a function of impeller diameter D, liquid physico-chemical properties (kinematic viscosity ν_L and density ρ_L), particle diameter d_p, density ρ_p and mass concentration of particles X:

$$N_c = S \cdot \nu_L^{0.1} \cdot \left[\frac{g(\rho_p - \rho_L)}{\rho_L}\right]^{0.45} \cdot X^{0.13} \cdot d_p^{0.2} \cdot D^{-0.85} \quad (1)$$

The value of the constant S is related to the geometry of the vessel and impeller. However, Ibrahim and Nienow (2004) have shown that, in the case of microcarrier suspension, the relation (1) may provide a 50% overestimation of N_c, probably due to the low density difference between liquid and microcarriers. Collignon et al. (2010) got further insight into microcarrier suspension by analyzing the liquid flow structure using Particle Image Velocimetry (PIV) measurements in a mechanically stirred vessel. Indeed, they compared the flow induced by seven designs of impellers, chosen among usual designs in animal cell culture processes and especially measured the power dissipation at the critical impeller agitation rate for microcarrier complete suspension. With this approach, the authors identified the TTP Mixel® and the Ear Elephant as two impeller designs minimizing the hydromechanical stresses encountered when complete suspension was reached. Furthermore, these authors showed that, for all impellers, the liquid velocity fields were globally similar at the critical agitation rate for particle complete suspension. Bioreactors agitated by an axial rotation of the impeller remain the most used systems for adherent-dependent cell cultures, especially because detailed knowledge can be found on their global characteristics (mixing time, hydromechanical stress, oxygen-liquid mass transfer), thus allowing a good scalability. Nevertheless, a major issue may arise from the use of air or oxygen sparging to ensure a sufficient amount of dissolved oxygen for cell respiration as it may lead to undesired foam or cell damage due to bubble burst at the gas-liquid free surface (Nienow, 2006).

Besides these usual culture systems, flasks shaken by an orbital motion have been revisited these last years for microbial and cell culture. Indeed, Büchs (2001) has estimated that more than 90% of all culture experiments in biotechnology are performed in shaken bioreactors. More recently, disposable bioreactors for animal cell culture in suspension mode, consisting in a cylindrical vessel shaken by an orbital motion, were shown as valuable systems in terms of mixing efficiency and oxygen transfer up to a scale of 1000 L (Stettler et al., 2007; Tissot et al., 2010; Zhang et al., 2009). An additional advantage of this mode of culture is the lack of damaging bubble bursts. Despite these new developments, surprisingly, concerning animal cell cultures on microcarriers, no data or correlation providing the critical agitation rate for complete suspension of microcarriers or, more generally of any kind of particles, are reported in the literature for shaken bioreactors.

In mechanically stirred vessels, the classic procedure to investigate liquid–solid suspensions consists in observing the vessel bottom. Although it has been intensively studied in the literature, the definition of particle suspension in these systems is still discussed (Zlokarnik, 2001). In shaken flasks, no standard protocol exists until now. As the shaking table is placed under the flask, the visualization of flask bottom would have required a modified shaking table, which would have been more complicated to handle. Therefore, the present study was devoted to investigate the microcarrier suspension in shaken flasks and, especially, to determine the critical agitation conditions (resulting from combined effects between agitation rate and orbital diameter) for microcarrier complete suspension as a function of the operating parameters (density of fluids and particles, viscosity, particle diameter and type). For that, a new protocol was first proposed to experimentally determine N_c for a given orbital shaking diameter. It was based on visual observations of blue-stained particle suspension obtained for 220 mixing conditions, changing flask design (Erlenmeyer flask or cylindrical flask) and size, liquid volume V_L, orbital shaking diameter d_0, liquid viscosity μ_L and density ρ_L, particle type, density ρ_P and diameter d_P. Most of the operating conditions were characteristic of animal cell culture at the laboratory scale. Some additional conditions were also considered to test the robustness of the model, for example by considering other solid particles than the microcarriers used for cell culture. Secondly, a dimensional analysis based on the knowledge of the physical mechanisms involved was performed, leading to a correlation relating a Froude number (in which the critical agitation rate N_c for particle complete suspension was embedded) to four other dimensionless numbers (including the ratio between the orbital shaken diameter and the flask diameter). Then, the critical agitation rates reported in this paper were analyzed and discussed with respect to the data available in the literature on the flow structure occurring inside the flask. At last, our results were used to identify the agitation conditions that promoted microcarriers suspension at a minimized power dissipation per unit of volume.

2. Material and methods

2.1. Shaken flasks and shaker

A bench top shaker Kühner LT-X placed in a temperature and CO_2 partial pressure controlled incubator was used (Kühner, Basel, Switzerland). The orbital shaking diameter d_0 was chosen equal to 1.25, 2.5 and 5 cm. Precisions of agitation rate and temperature measurements were ± 0.1 rpm and ± 0.3 °C respectively. Two geometries and various scales of shaken flasks were used. The first shape was widespread Erlenmeyer flask with a maximum liquid working volume V_T of 125, 250, 500, 1000 mL (Corning, USA) and 5000 mL (Duran, Germany). These systems have convex bottoms (Fig. 1). The second one consisted of glass straight cylindrical vessel with inner diameters of 2.4, 3.8, 4.5, 5.5, 8.7 and 11.5 cm. A schematic representation and detailed dimensions of Erlenmeyer flasks are given in Fig. 1 and in Table 1.

From Table 1, it can be observed that a degree of homothety existed between the Erlenmeyer flasks of different sizes. In particular, the following ratio was conserved whatever the flasks:

$$\frac{h_1}{d} = 1.17 \pm 0.07 \quad (2)$$

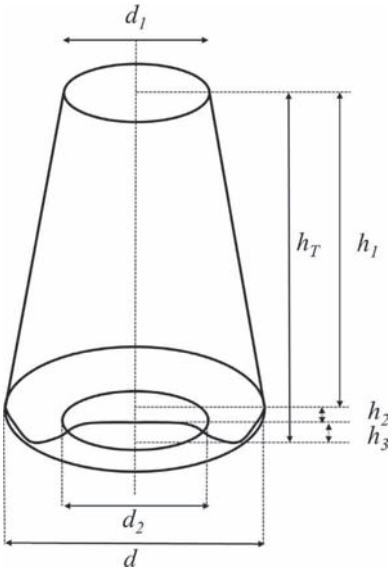

Fig. 1. Schematic representation of Erlenmeyer flask.

Table 1
Dimensions of Erlenmeyer flasks.

	Maximum liquid working volume V_T (mL)				
	125	250	500	1000	5000
d (cm)	6.6	8.3	10.1	12.8	22
d_1 (cm)	3.1	4.8	5.2	5.4	10.3
d_2 (cm)	4.2	4.9	6.6	6.6	14.4
h_1 (cm)	7.4	9.2	12.8	15.0	27.3
h_2 (cm)	0.4	1.1	1.5	2.2	1.7
h_3 (cm)	0.7	0.7	0.5	0.6	2.0

The other ratios (h_2/d; h_3/d; d_1/d and d_2/d), were not conserved from one flask to another:

$$0.42 < \frac{d_1}{d} < 0.58, \quad 0.06 < \frac{h_2}{d} < 0.17,$$
$$0.05 < \frac{h_3}{d} < 0.11, \quad 0.52 < \frac{d_2}{d} < 0.65 \qquad (3)$$

2.2. Fluids and liquid volume characterization

The fluid used in the present study was water either at 20 °C ($\mu_L = 1$ mPa s, $\rho_L = 1000$ kg m^{-3}) or at 37 °C ($\mu_L = 0.7$ mPa s, $\rho_L = 993$ kg m^{-3}) with similar density and viscosity to cell culture media. To get further insight in suspension mechanisms, the viscosity of the liquid was also increased by using aqueous solutions of CarboxyMethylCellulose (CMC, Fluka 21902) at a volume fraction of 1% (T=37 °C, $\rho_L = 999$ kg m^{-3}, $\mu_L = 20$ mPa s) and 0.3% (T=37 °C, $\rho_L = 999$ kg m^{-3}, $\mu_L = 6.5$ mPa s). Despite, in most cases, CMC solutions are expected to be non-newtonian (Ghnimi et al., 2008), the newtonian flow behavior of our CMC solutions was confirmed using rheological measurements on a double-Couette rheometer from TA instruments (New Castel, USA) (Fig. 2). It was also previously observed at the same concentrations by Pedersen et al. (1993). The range of shear rates is in agreement with the values obtained by Computational Fluid Dynamics numerical simulations of liquid flow in unbaffled shaken flasks by Mehmood et al. (2010).

Due to the facts that liquid volumes are practically and classically used during set-up of animal cell cultures in shaken flasks and that the determination of liquid height is more difficult

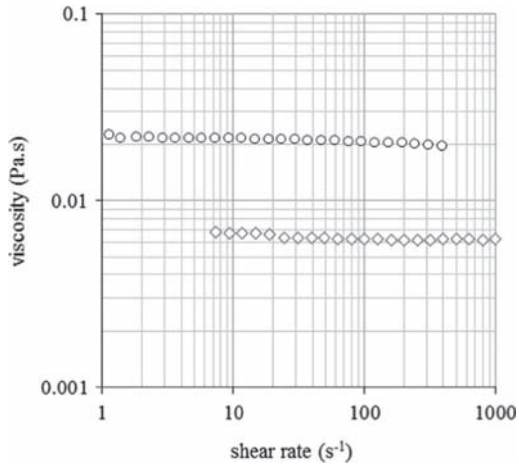

Fig. 2. Rheograms of medium-viscosity CMC solutions at a concentration of 0.3 (⋄) and 1% (○).

Table 2
Values of the ratio h_L/d for each filling ratio α for experiments in Erlenmeyer shaken flasks.

α (%)	Flask maximum working volume V_T (mL)				
	125	250	500	1000	5000
8	0.173	0.120	0.114	0.142	0.137
16	0.198	0.168	0.169	0.187	0.180
20	0.213	0.192	0.197	0.211	0.203
24	0.230	0.217	0.227	0.237	0.228
32	0.270	0.269	0.289	0.292	0.280
40	0.319	0.324	0.355	0.352	0.337
48	0.376	0.381	0.425	0.417	0.400
56	0.441	0.441	0.498	0.487	0.466
64	0.514	0.504	0.575	0.562	0.538
72	0.595	0.568	0.656	0.642	0.615
80	0.684	0.636	0.740	0.727	0.696

than liquid volume (convexity of Erlenmeyer flask bottoms), V_L has been chosen as the parameter characterizing the liquid phase domain for the dimensional analysis. For each Erlenmeyer flask, different liquid volumes V_L were thus tested and associated with different filling ratios of liquid, α, defined as $\alpha = V_L/V_T$, which varied between 0.08 and 0.8. In cylindrical flasks, the definition of total volume V_T is meaningless imposing rather the use of liquid height at rest h_L in the dimensional analysis. Indeed, as in classical agitated bioreactors, some authors (for instance Weheliye et al., 2013) measured the liquid height h_L instead of V_L, in shaken systems. In our opinion, the measurement of liquid volume is more precise than liquid height, especially in bench top culture systems. To make easier the comparison of our results with literature data, liquid heights at rest were also measured for each filling rate in Erlenmeyer flasks and ratios h_L/d calculated (Table 2). In cylindrical flasks, h_L/d varied from 0.2 to 0.7.

2.3. Characteristics of the particles

The particles used in the present study were either particles that are commonly used as animal cell microcarriers such as Cytodex-1 (GE Healthcare), Cytopore 2 (GE Healthcare) or Hillex (SoloHill), or not, such as Sephadex G10 and G25 (GE Healthcare), which were used to test the robustness of the model. Cytodex 1 are dextran beads with positive-charged DEAE groups throughout matrix. They are qualified of microporous. Molecules up to 100 000 molecular weight can enter these carriers, but the pores are not available for cells. Cytopore 2 are composed of cross-

linked cellulose with positive DEAE charges groups. With a pore size averaging 30 μm, their porosity is more than 90%. Like Cytodex 1, their surface is microporous to facilitate the cell adhesion, but their pores allow the entry of cells and protect them from shear forces. Hillex microcarriers are composed of polystyrene modified with a cationic amine which improves cell attraction. Solid and smooth construction prevents absorption of toxic byproducts. Sephadex are gel filtration media prepared by cross-linking dextran with epichlorohydrin. Different types of Sephadex differ in their degree of cross-linking and hence in their degree of swelling and their molecular fractionation range, from G-10 for small molecules to G-75 for larger molecules. For example the fractionation range of globular proteins is lower than 700 Da for Sephadex G-10 and between 1000 and 5000 Da for Sephadex G-25. As claimed by the supplier, the beads behave as rigid spheres obeying Darcy's Law. Pores are not available for cells.

For each of these particles, the hydrated mean Sauter diameter d_p were measured on 9 samples using laser diffraction technique (Mastersizer, Malvern, Worcestershire, UK) and standard deviations of particle size distributions were calculated. Diffraction data were collected and post-treated using a dedicated software (Mastersize, version 2.17). Particle density ρ_p was obtained from supplier data. Densities, mean diameters and surface properties of the particles are given in Table 3.

Thus, these particles exhibited a wide range of diameters, densities and structure properties but remained similar to cell culture microcarriers. The volume fraction of wet particles, defined as the ratio of wet particle total volume to liquid volume $\phi = V_P/V_L$, varied from 0.02 to 0.4 .

2.4. Experimental measurement of critical agitation rate for particle complete suspension

The method developed for measuring the critical agitation rate for particle complete suspension was based on a colorimetric technique. Side-view pictures from particle suspension and visual determination were used to identify critical agitation rate N_c, at a given d_0, by using a camera fixed on the orbital shaker using a clamp-like apparatus. To get enough image contrast between solid and liquid phases, wet particles were stained during 12 h using Trypan Blue and rinsed with fresh water. To determine N_c, agitation rate was first set to a low value for which particles remained settled on the bottom of the flask. Then, agitation rate was increased till N_c for which particles suspension was observed. Note that the homogeneous particle suspension was not considered in the present study: only the complete suspension state was investigated. An example of image acquisition, provided in Fig. 3, shows the impact of an increase in agitation rate on Cytodex-1 suspension in a 250 mL Erlenmeyer flask. To determine particle suspension, a 1 rpm step was applied to the shaker and N was maintained constant during 20 s approximately. The same procedure was repeated till complete suspension of particles was observed (Fig. 3D). Depending on the operating conditions, particle suspension suddenly moves from a completely settled state to a complete suspension state or exhibited an intermediate state characterized by a particles gathering in the centre of the flask (Fig. 3B and C) before complete suspension. Whatever the case, the transition from settled to completely suspended particles occurred within a few rpm, allowing an excellent precision for N_c determination.

3. Results

3.1. Establishment of the dimensionless correlation in Erlenmeyer flasks as a function of the filling ratio $\alpha = V_L/V_T$

As filling ratio is more adapted to Erlenmeyer flasks, the dimensional analysis methodology was first described in this case. The establishment of the dimensionless correlation based on h_L/d ratio for both cylindrical and Erlenmeyer flasks is proposed in Section 3.2.

The implementation of the dimensional analysis and the establishment of the dimensionless correlation consisted in three steps: (i) list of the physical quantities influencing the target variable N_c, (ii) establishment of the complete set of dimensionless numbers and (iii) determination of the process relationship linking N_c to the other dimensionless numbers.

3.1.1. List of the physical quantities influencing the target variable

The critical agitation rate for complete suspension, N_C, was chosen as target variable for dimensional analysis. As a first step, the physical quantities influencing N_c in Erlenmeyer flasks should be listed, verifying that these quantities were independent on one another. They could be then classified as follows:

1. The geometric parameters characterizing:
   - the shaker: this was the orbital diameter d_0,
   - the flask: they corresponded to the liquid filling ratio α, to the characteristic diameter of the Erlenmeyer flask d (see Fig. 1) and to other geometrical parameters, noted $\{p_{geo}\}$ with $\{p_{geo}\} = \{d_1, d_2, h_1, h_2, h_3\}$.
2. The material parameters related to the liquid phase (ρ_L, μ_L) and to the particles (ρ_p, d_p, particle volume fraction ϕ).
3. The gravity acceleration g.

Finally, the initial list of the physical quantities influencing the critical agitation rate for complete suspension in shaken flasks was

$$N_c = f(d_0, \alpha, d, \rho_L, \mu_L, \rho_p, d_p, \phi, g, \{p_{geo}\}). \quad (4)$$

3.1.2. Establishment of the complete set of dimensionless numbers

Fifteen parameters, which depended on three fundamental dimensions (mass – M, length – L and time – T), were involved in Eq. (4). They could be reduced, according to the Vachy–Buckingham theorem, to a relationship between $(15-3) = 12$ dimensionless numbers. Among them, three (equal to the number of fundamental dimensions) physical quantities (ρ_L, g and d) should be chosen as individual physical quantities (or as basis) to form the core matrix of the dimensional matrix, while the other ones would constitute the residual matrix (Table 4). This choice would of course impact the set of dimensionless numbers

Table 3
Characteristics of the hydrated particles.

Particle	Cytodex-1	Cytopore-2	Hillex	Sephadex G10	Sephadex G25
Density (kg m^{-3})	1030	1030	1100	1242	1093
Mean diameter (μm)	260 ± 120	306 ± 98	145 ± 40	86.5 ± 24	79 ± 32
Surface quality	Rough	Porous	Smooth	Porous	Porous
Porosity	Low (MW cut-off $< 100\,000$)	High (pore size = 30 μm)	No	Low (MW cut-off < 700)	Low (MW cut-off < 1000–5000)

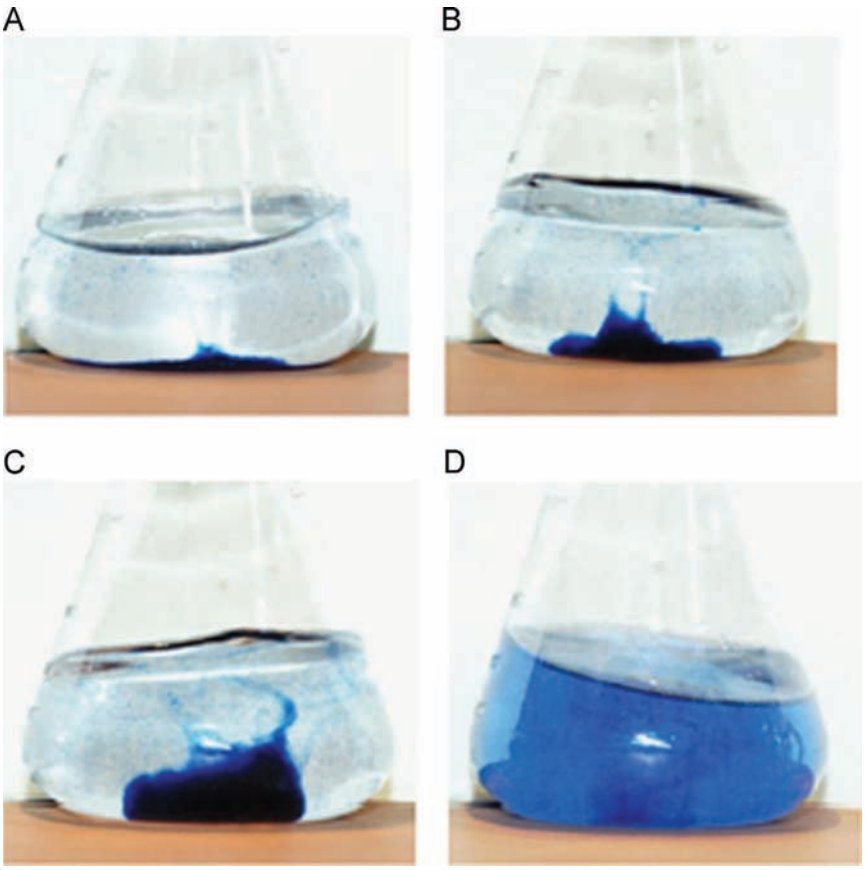

Fig. 3. The different steps leading to the complete suspension of Cytodex-1 microcarriers in a 250 mL Erlenmeyer flask. Operating conditions are V_L=120 mL, d_0=2.5 cm, and agitation rate: (A) N=110 rpm, (B) N=114 rpm, (C) N=116 rpm, and (D) N=120 rpm. Complete suspension was observed for N_c=120 rpm.

Table 4
Dimensional matrix of the physical quantities influencing N_c.

	Residual matrix								Core matrix		
	N_c	d_0	α	μ_L	ρ_p	d_p	ϕ	$\{p_{geo}\}$	g	ρ_L	d
Mass (M)	0	0	0	1	1	0	0	0	0	1	0
Length (L)	0	1	0	−1	−3	1	0	1	1	−3	1
Time (T)	−1	0	0	−1	0	0	0	0	−2	0	0

obtained, but Szirtes (2007) demonstrated that the sets associated with the different possible basis are equivalent from one to each other, as one set can be transformed into another one by matrix transformations. In Table 4, the columns were assigned to the individual physical quantities and the rows to the exponents related to their expression as a power product of the fundamental dimensions.

When transforming the core matrix into a unit matrix, a new residual matrix whose exponents were used to construct the dimensionless numbers was obtained (Table 5).

From the new residual matrix reported in Table 5, the following dimensionless ratios were constructed:

$$\pi_1 = \left(\frac{N_c}{\sqrt{g/d}}\right) = Fr_c, \quad \pi_2 = \left(\frac{d_0}{d}\right), \quad \pi_3 = \alpha,$$
$$\pi_4 = \left(\frac{\mu_L}{\rho_L \cdot g^{0.5} \cdot d^{1.5}}\right) = \mu^*, \quad \pi_5 = \left(\frac{\rho_p}{\rho_L}\right) = \rho^*$$
$$\pi_6 = \left(\frac{d_p}{d}\right), \quad \pi_7 = \phi, \quad \{\pi_{geo}\} \tag{5}$$

Table 5
New dimensional matrix obtained after transforming the core matrix into a unit matrix.

Residual matrix								Core matrix		
N_c	d_0	α	μ_L	ρ_p	d_p	ϕ	$\{p_{geo}\}$	g	ρ_L	d
0.5	0	0	0.5	0	0	0	0	1	0	0
0	0	0	1	1	0	0	0	0	1	0
−0.5	1	0	1.5	0	1	0	1	0	0	1

Thus, the dimensional analysis stated that the critical Froude number, Fr_c, in which the critical agitation rate N_c for particle complete suspension in flasks was embedded, was potentially affected by a minimum of 7 dimensionless numbers, describing respectively the effect of orbital shaking diameter (π_2), liquid filling ratio (π_3), liquid viscosity ($\pi_4 = \mu^*$), particle density ($\pi_5 = \rho^*$), particle diameter (π_6), volume fraction of particles ($\pi_7 = \phi$) and geometrical characteristics of the flasks $\{\pi_{geo}\}$.

3.1.3. *Determination of the process relationship predicting N_C*

Having no mechanistic indication on the mathematical form of the relationship linking Fr_c to the other dimensionless numbers, the simplest monomial form was looked for

$$Fr_c = \frac{N_c}{\sqrt{g/d}} = A \cdot \left(\frac{d_0}{d}\right)^{a_1} \cdot (\alpha)^{a_2} \cdot (\mu^*)^{a_3} \cdot (\rho^*)^{a_4} \cdot \left(\frac{d_p}{d}\right)^{a_5} \cdot (\phi)^{a_6} \cdot \prod_j \pi_{geo,j}^{a_j} \tag{6}$$

where

$$\prod_j \pi_{geo,j}^{a_j} = \left(\frac{d_1}{d}\right)^{a_7} \cdot \left(\frac{d_2}{d}\right)^{a_8} \cdot \left(\frac{h_1}{d}\right)^{a_9} \cdot \left(\frac{h_2}{d}\right)^{a_{10}} \cdot \left(\frac{h_3}{d}\right)^{a_{11}} \quad (7)$$

In Eq. (6), A was a constant and a_1, a_2,..., a_{11} were the exponents to which the dimensionless numbers were raised to. An optimization algorithm (non-linear GRC, Excel, Microsoft) was used to identify the constant and the different exponents of the preceding model by minimizing the following criterion for the N_{exp} experiments:

$$\beta = \frac{1}{N_{exp}} \sum_{i=1}^{N_{exp}} \left| \frac{Fr_{c,i}^{exp} - Fr_{c,i}^{mod}}{Fr_{c,i}^{exp}} \right| \quad (8)$$

$Fr_{c,i}^{exp}$ and $Fr_{c,i}^{mod}$ were the experimental and modeled values of Fr_c for experiment i respectively and N_{exp} is the number of experiments. To simplify the optimization algorithm, it has been chosen to directly include the influence of the geometrical dimensionless numbers into the initial constant of the monomial form, leading to

$$Fr_c = \frac{N_c}{\sqrt{g/d}} = A_{ef} \cdot \left(\frac{d_0}{d}\right)^{a_1} \cdot (\alpha)^{a_2} \cdot (\mu^*)^{a_3} \cdot (\rho^*)^{a_4} \cdot \left(\frac{d_p}{d}\right)^{a_5} \cdot (\phi)^{a_6} \quad (9)$$

with

$$A_{ef} = A \cdot \left(\frac{d_1}{d}\right)^{a_7} \cdot \left(\frac{d_2}{d}\right)^{a_8} \cdot \left(\frac{h_1}{d}\right)^{a_9} \cdot \left(\frac{h_2}{d}\right)^{a_{10}} \cdot \left(\frac{h_3}{d}\right)^{a_{11}} \quad (10)$$

Using experimental data obtained with Erlenmeyer flasks, the identification of the parameters led to model I (Eq. (11)) for the prediction of the critical Froude number Fr_c with a relative error of 4.2% (Fig. 4):

$$Fr_c = \frac{N_c}{\sqrt{g/d}} = 0.105 \cdot \left(\frac{d_0}{d}\right)^{-0.25} \cdot (\alpha)^{0.42} \cdot (\mu^*)^{0.01} \cdot (\rho^*)^{0.87} \cdot \left(\frac{d_p}{d}\right)^{-0.09} \cdot (\phi)^{0.002} \quad (11)$$

Noticing that, in Eq. (11), the exponents on dimensionless viscosity and volume particle fraction were low in comparison with the other exponents, the reduction of model I was then successfully tested by removing these two dimensionless numbers (model II, Eq. (12)) with a relative error of 4.2% (Fig. 5):

$$Fr_c = \frac{N_c}{\sqrt{g/d}} = 0.105 \cdot \left(\frac{d_0}{d}\right)^{-0.25} \cdot (\alpha)^{0.42} \cdot (\rho^*)^{1.0} \cdot \left(\frac{d_p}{d}\right)^{-0.07} \quad (12)$$

It can be noticed that the constants and the exponents of Eqs. (11) and (12) were very similar, which indicated that no physical information was lost when reducing Eq. (11).

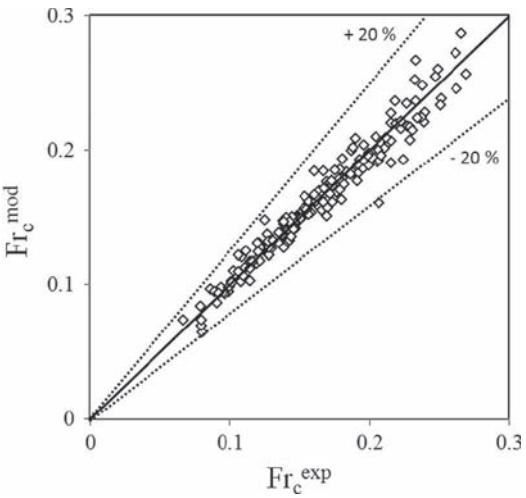

Fig. 4. Comparison of predicted (model I, Eq. (11)) and experimental critical Froude numbers Fr_c for experiments in shaken Erlenmeyer flasks.

For both models I and II, the ranges of operating conditions on which the models were proven valid in Erlenmeyer flasks were the following: $3.21 \times 10^{-6} < \mu^* < 4.96 \times 10^{-4}$; $1.01 < \rho^* < 1.24$; $6.62 \times 10^{-4} < d_p/d < 5.56 \times 10^{-3}$; $0.02 < \phi < 0.4$; $0.05 < \alpha < 0.8$; $0.058 < d_0/d < 0.91$; $0.42 < d_1/d < 0.58$; $0.52 < d_2/d < 0.65$; $1.1 < h_1/d < 1.24$; $0.06 < h_2/d < 0.17$; $0.05 < h_3/d < 0.11$; $0.067 < Fr_c < 0.27$.

Noticing that, by definition, $Fr_c \propto N_c \cdot d^{0.5}$ and that $Fr_c \propto (d_0/d)^{-0.25} \cdot (d_p/d)^{-0.075}$ (Eq. (12)), the scaling law of critical agitation rate for the complete suspension of given microcarriers, with respect to d_0 and d, would thus be in Erlenmeyer flasks:

$$N_c \propto d_0^{-0.25} \cdot d^{-0.18}. \quad (13)$$

3.2. Establishment of the dimensionless correlation in Erlenmeyer and cylindrical shaken flasks as a function of the h_L/d ratio

As previously exposed, it is possible to substitute the filling ratio α by the dimensionless liquid height (h_L/d) in Eqs. (11) and (12) using the data of Table 2 and the data related to cylindrical vessels.

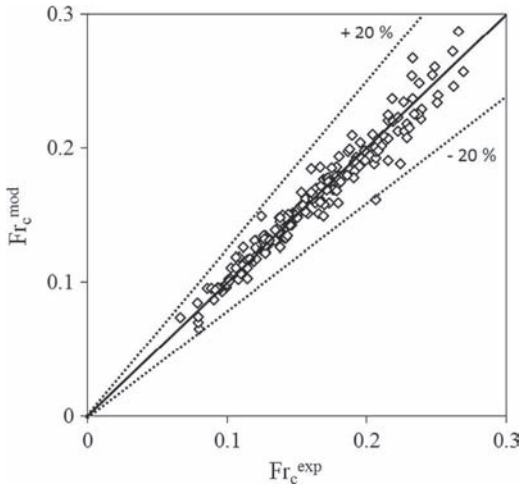

Fig. 5. Comparison of predicted (model II, Eq. (12)) and experimental critical Froude numbers Fr_c for experiments in shaken Erlenmeyer flasks.

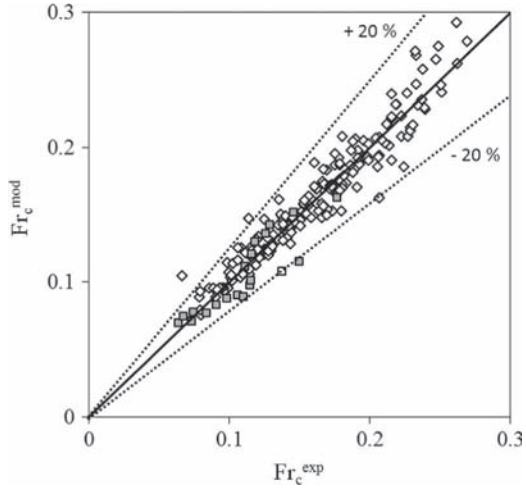

Fig. 6. Comparison of predicted (model III, Eq. (14)) and experimental critical Froude numbers Fr_c for experiments in shaken Erlenmeyer (◇) and cylindrical (■) flasks.

New data fitting led to Eq. (14) (model III) for both cylindrical and Erlenmeyer flasks (Fig. 6):

$$Fr_c = \frac{N_c}{\sqrt{g/d}} = A \cdot \left(\frac{d_0}{d}\right)^{-0.25} \cdot \left(\frac{h_L}{d}\right)^{0.49} \cdot (\rho^*)^{1.0} \cdot \left(\frac{d_p}{d}\right)^{-0.07} \quad (14)$$

The values of constant A and of relative error of model III were 0.12 and 5.7% for Erlenmeyer flasks and 1.39 and 10.2% for cylindrical flasks. Eq. (14) thus provides an equivalent scaling law to Eq. (13) despite a slight difference between the value of the exponent of h_L/d and α in these equations.

4. Discussion

4.1. Influence of operating parameters on Fr_c

Up to now, microcarrier suspension in shaken bioreactors was not studied in the literature. That is the reason why dimensional analysis, which is known as a robust tool for the description of complex phenomena, has been used in the present work. Our results demonstrated that the dimensionless numbers defining the flask geometry, the dimensionless viscosity and the particle volume fraction had small influence on the critical Froude number. As a consequence, particle suspension could be precisely characterized using a set of only 5 dimensionless numbers (Fr_c, d_0/d; ρ^*; d_p/d; α or h_L/d).

The impact of particle concentration on Fr_c was shown to be very low for the volume fraction of particles considered ($\phi < 0.4$); a similar trend is generally observed in mechanically stirred systems. When particles were not completely suspended, higher local concentrations of particles in the region of flask bottom could increase the apparent viscosity of the liquid. However, Eq. (11) revealed that an increase of liquid viscosity did not impact the critical agitation rate for particle complete suspension. To further discuss this low effect of liquid viscosity on particle suspension, the flow regime inside the flask for the range of operating conditions studied was determined. In the case of shaken flasks, Peter et al. (2006) proposed a criterion based on a flask Reynolds number defined as

$$Re = \frac{N \cdot d^2}{\nu_L} \quad (15)$$

For $Re > 60\,000$, flow regime was suggested to be turbulent whereas for lower values, flow was supposed laminar. The definition of this Reynolds number is nevertheless questionable, due to the choice of the characteristic linear velocity $N \cdot d$ which has an incomplete physical meaning for orbital shaken bioreactors. In classical stirred tank reactors, the characteristic linear velocity $N \cdot D$ (where D is the impeller diameter), which is proportional to the impeller tip speed ($\pi \cdot N \cdot D$), is generally used. Indeed, such a choice corresponds to the maximum linear velocity that an element of fluid could reach in the reactor. Based on this observation, Delaplace et al. (2007) defined, for planetary mixers, a characteristic linear velocity whose analytical expression (deduced from the instantaneous kinematics of a point located at the end of the tip) integrated the combination of both rotation and gyration movements of the mixer. These authors then used this consistent linear velocity to define the Reynolds number. Thus, in our case, the velocity ($N \cdot d_0$) should rather be used in the definition of the Reynolds number, as suggested by Kato et al. (1996).

Using Eq. (15) anyway, the Reynolds numbers remained lower than 50 000 for all of our experiments, which would indicate a non-fully turbulent regime. Thus, the low impact of liquid viscosity on the critical agitation rate for particle suspension could not be due to the occurrence of a fully turbulent flow inside the flasks, as generally admitted in conventional mechanically stirred vessels. Nevertheless, in our opinion, such considerations should be taken with caution.

The interactions between particles and flask walls, described by the dimensionless ratio d_p/d remained weak, as indicated by the low fitted values of the exponent (-0.07). Similarly to mechanically stirred reactors, the major contribution of particles on the critical agitation rate came from the ratio of particle to liquid densities and from the filling ratio (α or h_L/d) which impacted the relative effect of gravity and buoyancy forces.

4.2. Particle suspension and shaken flask hydrodynamics

In a general point of view, particle suspension should be linked to liquid velocity fields, especially at the critical agitation rate. Indeed, using Particle Image Velocity measurements, Collignon et al. (2010) revealed that, at the particle complete suspension, the velocity fields obtained using various impeller designs in a mixing vessel were very similar. Recently, Weheliye et al. (2013) provided a thorough characterization of the flow and mixing dynamics in a cylindrical shaken bioreactor thanks to phase-resolved PIV measurements. In particular, they showed that the transport phenomena were controlled by the occurrence of either two counter rotating vortices or a vertical vortex rotating around the flask axis. In the first case, which corresponded to the in-phase flow regime, these authors demonstrated that two counter-rotating vortices took source near the free surface, progressively reached the flask bottom and disappear when increasing the agitation rate. The free surface shape remained mainly two-dimensional. In the second case, occurring for higher rotation rates, the so-called out-of-phase regime appeared, characterized by a phase delay between the interface orientation and the shaker table position. A vortex with a vertical axis was then formed on the side of the bioreactor opposite to the highest side of the free surface (Weheliye et al., 2013).

From these observations, the same authors established a scaling law predicting the transitional agitation rate from the in-phase to the out-of-phase regimes. It was based on the analysis of the free surface motion (the driving mechanism in a shaken bioreactor) and, in particular, the maximum inclination and dimensionless wave amplitude of the free surface. Depending on the dimensionless fluid height h_L/d, this scaling law was differently expressed.

- If $h_L/d < (d_0/d)^{0.5}$, Weheliye et al. (2013) showed that the Froude number Fr_a related to the regime transition depends on the ratio h_L/d and on the orbital to flask diameters ratio d_0/d, such as

$$Fr_a = \frac{2(\pi \cdot N)^2 \cdot d_0}{g} = \left(\frac{1}{a_0}\right) \cdot \left(\frac{h_L}{d}\right) \cdot \left(\frac{d_0}{d}\right)^{0.5} \quad (16)$$

  where a_0 was given equal to 1.4 for water at 20 °C. In this case, the two counter-rotating vortices were found to effectively reach the flask bottom. It is interesting to observe that these three ratios were comparable to the ones established in Model II (Eq. (12)) when considering only the liquid phase characteristics.
- If $h_L/d > (d_0/d)^{0.5}$, Weheliye et al. (2013) showed that the scaling law involved only the Froude number Fr_r:

$$Fr_r = \frac{2(\pi \cdot N)^2 \cdot d}{g} = \left(\frac{1}{a_0}\right) \quad (17)$$

From a fluid mechanics point of view, it is relevant to suppose that particle suspension should efficiently took place at the transition between these two regimes, especially when the two

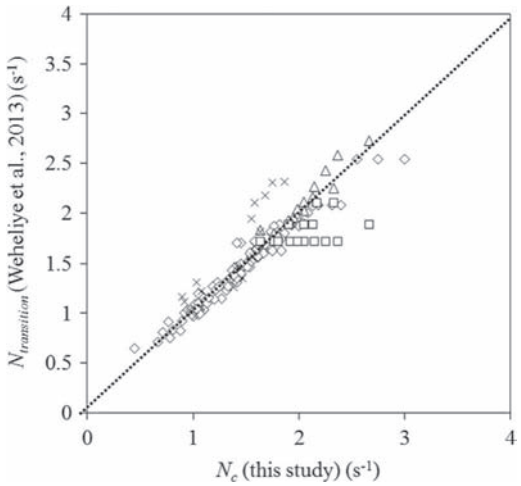

Fig. 7. Comparison of experimental critical agitation rates in shaken Erlenmeyer flasks (this work) with agitation rates characteristic of flow regime transitions in shaken cylinders (Weheliye et al., 2013). (◇) $h_L/d < (d_0/d)^{0.5}$ and Eq. (16); (△) $h_L/d > (d_0/d)^{0.5}$ and Eq. (16); (□) $h_L/d > (d_0/d)^{0.5}$ and Eq. (17). Comparison between experiments in cylindrical flasks and predictions of Eq. (16) are also given (×). Experimental data of N_c was here restricted to Cytodex-1 microcarriers suspension.

counter-rotating vortices reached the bioreactor bottom. For this reason, we have compared our experimental agitation rates for particle complete suspension to the transition agitation rate predicted by Eqs. (16) or (17). We should keep in mind that Weheliye et al. (2013) performed their experiments in cylindrical shaken bioreactors only, and not in shaken Erlenmeyer flasks. This comparison was reported in Fig. 7 for Cytodex-1 microcarrier. A good agreement was obtained when Eq. (16) was used, even for the operating conditions corresponding to $h_L/d > (d_0/d)^{0.5}$. This comparison remained satisfactory when applied to our experiments in cylindrical flasks (Fig. 7).

This was confirmed by considering the critical Froude number defined in Eq. (5) which could be related to the axial Froude number defined in Eq. (16), such as

$$Fr_c = \frac{N_c}{\sqrt{g/d}} \propto Fr_a^{0.5} \left(\frac{d_0}{d}\right)^{-0.5} \tag{18}$$

By introducing Eq. (16) in Eq. (18), we obtained

$$Fr_c \propto \left[\left(\frac{h_L}{d}\right) \cdot \left(\frac{d_0}{d}\right)^{0.5}\right]^{0.5} \cdot \left(\frac{d_0}{d}\right)^{-0.5} = \left(\frac{h_L}{d}\right)^{0.5} \cdot \left(\frac{d_0}{d}\right)^{-0.25} \tag{19}$$

As previously shown (Eq. (14)), the dimensional analysis has predicted

$$Fr_c \propto \left(\frac{h_L}{d}\right)^{0.49} \cdot \left(\frac{d_0}{d}\right)^{-0.25} \tag{20}$$

An excellent agreement was thus observed between our model (Eq. (12)) and the scaling law proposed by Weheliye et al. (2013) for regime transition (Eq. (16)). These results would suggest that the mechanisms controlling the complete suspension of particles in shaken flasks were related to regime transition and, especially, to the occurrence of the two counter-rotating vortices reaching the flask bottom.

4.3. Suspending particles at lower power dissipation per unit of volume

When suspended in bioreactors, microcarriers and the cells adhered on their surface are subjected to hydrodynamic stresses arising from cell-turbulence interactions or collisions between microcarriers (Cherry and Papoutsakis, 1988). The consequences are cell damage on the microcarriers or cell detachment that can lead to a rapid cell lysis and, consequently, to a decrease of process productivity. In a fully turbulent flow, a commonly used theory states that cell damage mainly occurs when the Kolmogorov length scale becomes lower than the microcarrier characteristic size. This length scale is directly related to the turbulent dissipation rate ε. Considering a mean value for the Kolmogorov scale in the mixing vessel $\langle l_K \rangle$, the power dissipation per unit of volume P/V can be related to the mean value of the turbulent dissipation rate $\langle \varepsilon \rangle = P/(\rho_L V_L)$ and thus to $\langle l_K \rangle$:

$$\langle l_K \rangle = \left(\frac{\nu_L^3}{\langle \varepsilon \rangle}\right)^{0.25} \tag{21}$$

However, the physical meaning of this theory is still discussed (Nienow, 2006). Moreover, as mentioned earlier, when basing on the definition of the Reynolds number given in Eq. (15), the flow encountered during our experiments would be not fully turbulent. If this is confirmed, it would limit even more the relevancy of the preceding Kolmogorov theory in the present study performed in shaken flask.

That is why a criterion based on the minimization of the power dissipation per unit of volume at the complete suspension state appears at present as the best strategy for the scale-up of microcarrier-based culture processes (Nienow, 2006). In unbaffled Erlenmeyer flasks, power dissipation was provided by Büchs et al. (2000):

$$Ne' = 70 \cdot Re^{-1} + 25 \cdot Re^{-0.6} + 1.5 \cdot Re^{-0.2} \tag{22}$$

with the modified Newton and Reynolds numbers defined by

$$Ne' = \frac{P}{\rho_L \cdot N^3 \cdot d^4 \cdot V_L^{1/3}}, \quad Re = \frac{\rho_L \cdot N \cdot d^2}{\mu_L} \tag{23}$$

Thus, in Erlenmeyer flasks, the power dissipation per unit of volume did not depend on the orbital diameter d_0. This was not the case in cylindrical vessels as shown by a recent study in which a relationship was proposed to predict the power dissipation in cylindrical vessels shaken by an orbital motion (Klöckner et al., 2012):

$$Ne = 9 \cdot Re^{-0.17} \cdot \left(\frac{V_L}{d^3}\right)^{0.44} \cdot \left(\frac{N^2 \cdot d_0}{g}\right)^{0.42} \tag{24}$$

with the Newton and Reynolds numbers defined by

$$Ne = \frac{P}{\rho_L \cdot N^3 \cdot d^5}, \quad Re = \frac{\rho_L \cdot N \cdot d^2}{\mu_L} \tag{25}$$

Eq. (24) was proven to be valid for $2400 < Re < 250\,000$, $0.004 < (N^2 \cdot d_0)/g < 0.12$, $0.085 < V_L/d^3 < 0.5$ and when liquid motion was induced in the cylindrical flask, i.e. for mixing conditions with $Fr_a > 0.28 \cdot \left(V_L/d^3\right) \cdot (d_0/d)$. This latter condition, and especially the value of the constant 0.28, was verified for vessel sizes between 10 and 2000 L, which were significantly bigger than the volumes tested in the present study. However, the values of Reynolds numbers, axial Froude and ratio V_L/d^3 calculated for our experiments in cylindrical flasks were in the validity range of Eq. (24).

The calculations of power dissipation per unit of volume in shaken flasks by using Eq. (22) revealed that power dissipation was slightly correlated with the critical Froude number (Fig. 8). Thus, a reduction of power dissipation to reach particle suspension could be achieved by reducing Froude number. That means that the use of large orbital shaking diameter is beneficial to the minimization of the power dissipation required for particle complete suspension. Furthermore, the impact of flask size on power dissipation at a given Froude number was not sensible, thus

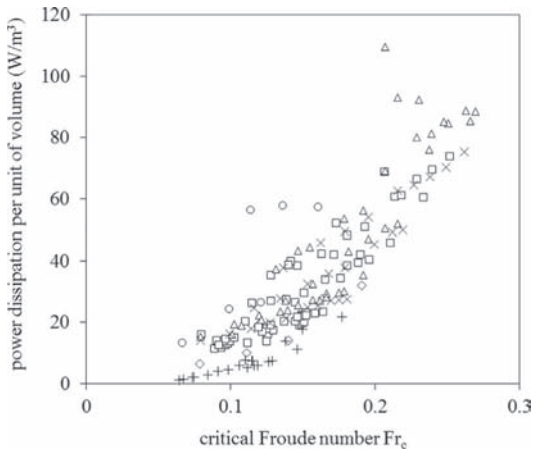

Fig. 8. Predictions of power dissipation per unit of volume in shaken Erlenmeyer flasks and cylinders in function of the experimental critical Froude number using Eqs. (22) and (24) respectively. Experiments with microcarriers (Cytodex-1, Hillex, Cytopore-2). Shaken flasks (◇) V_T=125 mL, (□) V_T=250 mL, (△) V_T=500 mL, (×) V_T=1000 mL, (○) V_T=5000 mL. Cylindrical vessel (+).

indicating a good scalability of power dissipation per unit of volume required for particle suspension, when vessel size increases. Using the 5 cm orbital diameter, the range of power dissipation calculated in Erlenmeyer flasks remained similar to the values generally encountered in mechanically stirred bioreactors, around 20 W m^{-3} (Nienow, 2006). It is worthwhile noticing that the use of cylindrical vessels promoted lower dissipations per unit of volume, around 10 W m^{-3} at the critical agitation conditions, suggesting that this vessel geometry should be preferentially chosen for microcarrier cell culture. These values were close to the ones reported at the complete suspension state in mechanically stirred bioreactors: Ibrahim and Nienow (2004) measured a power dissipation of approximately 1 W m^{-3} for a 45° pitched blade turbine and a Chemineer HE-3 hydrofoil while Collignon et al. (2010) reported values of 0.3 W m^{-3} and 1.8 W m^{-3} for ear-elephant and A315 impellers respectively.

However, an important difference between stirred and shaken bioreactors may arise from the flow regime expected in the vessel. Indeed, the flow regime encountered may impact the heterogeneity of the hydromechanical stresses inside the bioreactor and thus the validity of the use of a global power dissipation per unit of volume P/V as a valuable criterion to predict possible hydrodynamic damage of microcarriers. In unbaffled Erlenmeyer shaken flask, Peter et al. (2006) showed that in the laminar/transition regime ($Re < 60\,000$), it could be assumed that the maximum value of dissipation rate was similar to the mean value $\varepsilon_{max} \approx \langle\varepsilon\rangle$. Conversely, in mechanically stirred bioreactors operating at the fully turbulent flow regime at the complete suspension state, a ten-fold increase of turbulent dissipation rate could be expected in the impeller region, for example for pitched-blade turbines (Gabriele et al., 2009). Finally, unbaffled shaken bioreactors could be valuable systems for suspending microcarriers at low hydromechanical stress levels.

5. Conclusion

Shaken flasks are widely used in animal cell culture, especially at the laboratory scale. While these systems have been intensively characterized in terms of power dissipation, oxygen mass transfer and mixing times, no data concerning particle suspension, and in particularly microcarriers, could be found in the literature. To fill this lack, our study proposed, on the basis of experiments and a dimensional analysis, a relationship predicting the critical agitation conditions required to ensure particle suspension in Erlenmeyer and cylindrical shaken flasks, with an excellent accuracy. The present work thus revealed that these critical conditions were mainly a function of the particle to liquid densities ratio, the geometry ratio d_0/d, the flask filling ratio α and, to a lesser extent, of the particle to flask diameter ratio. Moreover, using literature data, a link between particle suspension and the transition from in-phase to out-of-phase regime characterized by the occurrence of two counter-rotating vortices reaching the flask bottom was suggested. Finally, shaken and, especially, cylindrical flasks, could be valuable systems for cell culture on microcarriers, as indicated by the levels of power dissipation per unit of volume calculated at the critical agitation rate required for particle complete suspension. Future work is provided to build a physical model characterizing flask hydrodynamics at complete particle suspension, for example by performing numerical simulations of the liquid–solid flow encountered.

Nomenclature

a_i ($i=1\ldots11$)	model constants (dimensionless)
α	filling ratio (dimensionless)
β	optimization criterion (dimensionless)
d	maximal flask diameter (Fig. 1) (m)
d_p	mean particle diameter (m)
d_0	orbital shaking diameter (m)
d_1	flask dimension (Fig. 1) (m)
d_2	flask dimension (Fig. 1) (m)
D	impeller diameter (m)
ε	turbulent dissipation rate (m^2 s^{-3})
Fr_a	axial Froude number (Eq. (16)) (dimensionless)
Fr_c	critical Froude number for microcarrier complete suspension (Eq. (5)) (dimensionless)
Fr_r	radial Froude number (Eq. (17)) (dimensionless)
g	gravity constant (m s^{-2})
h_1	flask dimension (Fig. 1) (m)
h_2	flask dimension (Fig. 1) (m)
h_3	flask dimension (Fig. 1) (m)
h_L	liquid height at rest (m)
h_T	liquid height at maximum working volume (m)
l_K	Kolmogorov scale (m)
μ_L	dynamic liquid viscosity (Pa s)
μ^*	dimensionless viscosity (dimensionless)
N	agitation rate (s^{-1})
N_c	critical agitation rate for particle complete suspension (s^{-1})
N_{exp}	number of experiments (dimensionless)
Ne	Newton number (dimensionless)
Ne'	modified Newton number (dimensionless)
ν_L	kinematic liquid viscosity(m^2 s^{-1})
P	power dissipation (W)
π_i ($i=1\ldots7$)	dimensionless numbers (dimensionless)
P/V	power dissipation per unit of volume (W m^{-3})
ϕ	volume fraction of particles (dimensionless)
Re	Reynolds number (dimensionless)
ρ^*	dimensionless density (dimensionless)
ρ_L	liquid density (kg m^{-3})
ρ_p	particle density (kg m^{-3})
S	Zwietering constant (Eq. (1)) (dimensionless)
T	temperature (K)
V_L	liquid volume (m^3)
V_T	maximum liquid working volume (m^3)
V_P	particle total volume (m^3)
X	mass concentration of particles (kg m^{-3})

Acknowledgments

The authors would like to sincerely thank Sabrina Bettray and Fabrice Blanchard for their valuable technical contribution and Professor Rachid Raouhadj for his scientific expertise.

References

Büchs, J., 2001. Introduction to advantages and problems of shaken cultures. Biochem. Eng. J. 7 (2), 91–98.

Büchs, J., Maier, U., Milbradt, C., Zoels, B., 2000. Power consumption in shaking flasks on rotary shaking machines. II. Nondimensional description of specific power consumption and flow regimes in unbaffled flasks at elevated liquid viscosity. Biotechnol. Bioeng. 68 (6), 594–601.

Cherry, R.S., Papoutsakis, E.T., 1988. Physical mechanisms of cell damage in microcarrier cell culture bioreactors. Biotechnol. Bioeng. 32 (8), 1001–1014.

Collignon, M.-L., Delafosse, A., Crine, M., Toye, D., 2010. Axial impeller selection for anchorage dependent animal cell culture in stirred bioreactors: methodology based on the impeller comparison at just-suspended speed of rotation. Chem. Eng. Sci. 65 (22), 5929–5941.

Delaplace, G., Thakur, R.K., Bouvier, L., André, C., Torrez, C., 2007. Dimensional analysis for planetary mixer: mixing time and Reynolds numbers. Chem. Eng. Sci. 62 (5), 1442–1447.

Ferrari, C., Balandras, F., Guedon, E., Olmos, E., Chevalot, I., Marc, A., 2012. Limiting cell aggregation during mesenchymal stem cell expansion on microcarriers. Biotechnol. Prog. 28 (3), 780–787.

Gabriele, A., Nienow, A., Simmons, M., 2009. Use of angle resolved {PIV} to estimate local specific energy dissipation rates for up- and down-pumping pitched blade agitators in a stirred tank. Chem. Eng. Sci. 64 (1), 126–143.

Ghnimi, S., Flach-Malaspina, N., Dresch, M., Delaplace, G., Maingonnat, J., 2008. Design and performance evaluation of an ohmic heating unit for thermal processing of highly viscous liquids. Chem. Eng. Res. Des. 86 (6), 626–632.

Ibrahim, S., Nienow, A., 2004. Suspension of microcarriers for cell culture with axial flow impellers. Chem. Eng. Res. Des. 82 (9), 1082–1088.

Kato, Y., Hiraoka, S., Tada, Y., Koh, S., Lee, Y., 1996. Mixing time and power consumption for a liquid in a vertical cylindrical vessel, shaken in a horizontal circle. Chem. Eng. Res. Des. 74 (4), 451–455.

Klöckner, W., Tissot, S., Wurm, F., Büchs, J., 2012. Power input correlation to characterize the hydrodynamics of cylindrical orbitally shaken bioreactors. Biochem. Eng. J. 65, 63–69.

Mehmood, N., Olmos, E., Marchal, P., Goergen, J.-L., Delaunay, S., 2010. Relation between pristinamycins production by *Streptomyces pristinaespiralis*, power dissipation and volumetric gas-liquid mass transfer coefficient, k_{la}. Process Biochem. 45 (11), 1779–1786.

Nienow, A.W., 2006. Reactor engineering in large scale animal cell culture. Cytotechnology 50 (1–3), 9–33.

Pedersen, A.G., Bundgaard-Nielsen, M., Nielsen, J., Villadsen, J., Hassager, O., 1993. Rheological characterization of media containing penicillium chrysogenum. Biotechnol. Bioeng. 41 (1), 162–164.

Peter, C.P., Suzuki, Y., Buchs, J., 2006. Hydromechanical stress in shake flasks: correlation for the maximum local energy dissipation rate. Biotechnol. Bioeng. 93 (6), 1164–1176.

Stettler, M., Zhang, X., Hacker, D.L., deJesus, M., Wurm, F.M., 2007. Novel orbital shake bioreactors for transient production of CHO derived IgGs. Biotechnol. Prog. 23 (6), 1340–1346.

Szirtes, T., 2007. Applied Dimensional Analysis and Modeling. Butterworth-Heinemann, Oxford, United Kingdom.

Tissot, S., Farhat, M., Hacker, D.L., Anderlei, T., Kuhner, M., Comninellis, C., Wurm, F., 2010. Determination of a scale-up factor from mixing time studies in orbitally shaken bioreactors. Biochem. Eng. J. 52 (2–3), 181–186.

Weheliye, W., Yianneskis, M., Ducci, A., 2013. On the fluid dynamics of shaken bioreactors-flow characterization and transition. AIChE J. 59 (1), 334–344.

Zhang, X., Bürki, C.-A., Stettler, M., De Sanctis, D., Perrone, M., Discacciati, M., Parolini, N., DeJesus, M., Hacker, D.L., Quarteroni, A., Wurm, F.M., 2009. Efficient oxygen transfer by surface aeration in shaken cylindrical containers for mammalian cell cultivation at volumetric scales up to 1000 L. Biochem. Eng. J. 45 (1), 41–47.

Zlokarnik, M., 2001. Stirring: Theory and Practice. Wiley-VCH, Weinheim, Germany.

Zwietering, T., 1958. Suspending of solid particles in liquid by agitators. Chem. Eng. Sci. 8 (3-4), 244–253.